

Fractional and simultaneous precipitation: recovering critical metals from multicomponent solutions

Andressa Mazur, Frederico Marques Penha (✉)

Division of Resource Recovery, Department of Chemical Engineering, KTH Royal Institute of Technology, Stockholm 114 28, Sweden

© The Author(s) 2025. This article is published with open access at link.springer.com and journal.hep.com.cn

Abstract This study explores fractional and simultaneous precipitation methods to recover metals from a synthetic solution containing the major components from lithium-ion battery recycling leachates: Co, Ni, Mn, Li, and H₂SO₄. Thermodynamic simulations analyzed the behavior of the metal-bearing solutions during hydroxide precipitation to guide process design. The fractional precipitation process was divided into three steps: pH-adjustment (D1), Co and Ni recovery (D2), and Mn recovery (D3). D2 achieved 89.7% Ni and 76.8% Co recovery; alongside Mn and Li were also removed (15% and 25% respectively). D3 showed mainly Mn recovery (68%) along with 18.7% Co and 7.3% Ni. Simultaneous precipitation resulted in over 99.7% recovery of Co, Ni, and Mn, with a small amount of Li (15%) being recovered from the solution. Na removal from the solution was observed across all experiments. X-ray diffraction analysis revealed that the phases formed were distinct from the predictions. Regardless of the presence of NH₄OH as a chelating agent in solution, a mixed nickel-cobalt-manganese oxide could be obtained after calcination. This approach offers a potentially less laborious method for recovering metals in products relevant to cathode precursors in a single step from recycling leachate.

Keywords fractional precipitation, simultaneous precipitation, multicomponent systems, LIB recycling, thermodynamic simulation

1 Introduction

Lithium-ion battery (LIB) recycling is highly relevant, especially in Europe, where Li and other metals contained in LIBs (Co, Mn, and Ni) were categorized as critical raw

materials for societal development by the European Union [1,2]. The typical LIB recycling process consists of a hydrometallurgical process based on dissolving metallic components by leaching using inorganic acids (H₂SO₄ or HCl) and reducing agents (e.g., H₂O₂). After leaching, the most common separation methods used are solvent extraction (SX), ion exchange, electrochemical deposition, crystallization, and precipitation, often used in various combinations [1,3]. SX is the state-of-the-art method for recovering transition metals like Ni, Co, and Mn from leachates, using extractants such as di-(2-ethylhexyl) phosphoric acid, organophosphorus acids (e.g., Cyanex 272), and chelating oximes [1] in pure solutions for further precipitation as metal salts. While highly effective and commercially viable, SX's multi-stage nature results in notable drawbacks, including metal losses, high costs, and extended processing times. Furthermore, repeated cyclic operations generate hazardous organic waste, along with acidic and alkaline wastewater, creating environmental challenges due to secondary pollution [4–7].

Precipitation is a traditional method for recovering metals with high purity in hydrometallurgy. It is widely applied in the industry due to the low cost and simplicity of the process [8]. Hydroxides, sulfides, carbonates, and arsenates are often used as precipitants in the recovery of metals [9]. Literature reports crystallization and precipitation routes to the recovery of Co in the form of carbonate [10,11], oxalate [12–16], phosphate [17], hydroxide [18,19], and oxide [20]. Ni can be recovered as carbonate [14,19], hydroxide [20], and nickel dimethylglyoxime [16,18]. Mn is reported to be recovered as permanganate [18,21], oxide [13], carbonate [14,19], sulfide, or Ni-Co-Mn sulfide [22], and mixtures of manganese oxides using sodium hypochlorite [10]. Li is mainly recovered as a carbonate—widely applied in the industry—using sodium carbonate or carbon dioxide, usually as the final step of the recycling process [11,14,16,18,21,23–25]. However, it can also be

recovered as fluoride [12], sulfate [26], or phosphate [27]. Under the appropriate conditions, up to 99% recovery of cobalt and lithium can be reached [1,28].

Hydroxide precipitation is well-known and the most common in the production of NMC (nickel manganese cobalt) cathodes by coprecipitation. In this process, Co, Ni, and Mn sulfates are dissolved in water and precipitated in the presence of a chelating agent, usually ammonium hydroxide [29–32]. The product is a dense single-phase spherical particle $\text{Ni}_x\text{Mn}_y\text{Co}_{1-x-y}(\text{OH})_2$. The lithiation process follows with the mixing of Li salts with the precursor NMC before the calcination, resulting in the LIB cathode, NMC11 ($\text{Li}[\text{Ni}_{0.33}\text{Mn}_{0.33}\text{Co}_{0.33}]\text{O}_2$), one of the most promising candidates for industrial application [29,31,33,34]. Many articles reported that this material has a good tap density, a key property for battery materials that affect the packing density of the active material in electrodes, influencing the performance and efficiency of LIBs, and is capable of retaining the initial capacity for longer charge-discharge cycling, with a focus on different aspects of this material production, such as synthesis process [30,33,35–38], material characterization [38–41], presence of defects and uniformities in the material [35,42,43], and regeneration from recycling streams [31,33,34,44–47].

Although crystallization and precipitation are well-established and widely studied techniques for single component solutions, when dealing with multicomponent solutions, different parameters come into play. The presence of additional solutes significantly alters the system's behavior, frequently leading to reduced purity and increased crystallite mismatches due to complex interactions among the various solutes and solvents [48,49]. Most crystallization strategies are designed to recover a single compound from such mixtures, with limited efforts directed toward promoting the simultaneous formation of multiple distinct crystalline phases [49]. Some approaches that focus on recovering multiple compounds include simultaneous precipitation (SP) and fractional precipitation (FP).

SP aims for the recovery of different compounds in separated phases, ideally in a one-step operation, using strategies that promote a good purity level and separation of crystals from different compounds—avoiding the formation of polycrystalline particles with mixed composition and cocrystals. SP was investigated by Penha et al. [49], who propose a seeding strategy that allows the crystallization of NaCl and KCl simultaneously from solution and downstream mechanical separation in two distinct populations by sieving. In parallel, in FP, also known as sequential precipitation, an order of precipitation enables the recovery of different compounds using highly selective precipitant agents and solution conditions, such as pH variation and antisolvent addition. FP is reported in the literature applied to the recovery of metals from salt brines [50], lateritic ores [51], battery recycling process

[14,52], and acid mine drainage [53], among other waste streams [54–56].

The design of simultaneous and fractional precipitation processes requires an understanding of the singularities of each multicomponent system, the study of phase equilibria, and the thermodynamic conditions. Hence, thermodynamic simulations are widely used in the field of precipitation [9,57–60]. Software such as OLI Studio [61], PHREEQC [62], HYDRA, and MEDUSA [63] have an extensive database of thermodynamic information to enable the simulation of single and multi-component systems to improve separation process design. Still, significant effort is needed to bridge the gap between thermodynamic modeling and experimental approaches for studying simultaneous and fractional precipitation in multicomponent solutions.

To define the composition of the synthetic leachate to be applied in this work, a literature review was conducted, targeting studies on leachates obtained from the sulfuric acid leaching of spent NMC-type LIBs. Relevant publications were examined and summarized in Table 1, considering variables such as metal ion concentrations, sulfuric acid molarity, presence of reducing agents, solid-to-liquid ratio, and temperature.

While the metal concentrations reported in the literature varied widely, most studies focused on Li^+ , Co^{2+} , Ni^{2+} , and Mn^{2+} as the primary components, with some including a pretreatment step to remove impurities [19,73,74]. However, the variability in reported values prevented the establishment of representative average concentrations across the data set. Therefore, the concentrations for this study were instead based on electric vehicles NMC-type LIB waste leached under the following conditions (unpublished data): solid-to-liquid ratio of 1:10 $\text{g}\cdot\text{mL}^{-1}$, 2 $\text{mol}\cdot\text{L}^{-1}$ H_2SO_4 , 3% v/v H_2O_2 (59% w/w), and 50 °C for 60 min. Li, Co, Ni, and Mn are the predominant metal ions in the resulting leachate, while Cu and Al were present in minor amounts and Zn, Mg, Fe, K, and Na were detected only in trace amounts, thus were left out of the synthetic leachate for this study.

In this context, this study explores the potential of FP and SP as efficient alternatives to conventional LIB recycling methods. While precipitation methods for individual metal recovery have been widely reported [12–16], to the best of our knowledge, no study directly compares FP and SP in multicomponent systems. Using NaOH as a precipitant and guided by thermodynamic simulations, we explored the possibility of selectively recovering Co, Ni, and Mn from a synthetic solution in the same concentrations found in a LIB leachate. Laboratory-scale experiments were used to assess the effectiveness and selectivity of each method, to which solid products and final solutions were characterized. The observed results were compared with simulation predictions to identify discrepancies, particularly related to co-precipitation, impurity incorporation, and phase

Table 1 NMC battery leachate composition in literature

Composition (g·L ⁻¹)							L/S ratio (mL·g ⁻¹)	Temperature (°C)	Time (min)	H ₂ SO ₄ (mol·L ⁻¹)	Reducing agent vol % H ₂ O ₂	Ref.
Co	Li	Mn	Ni	Fe	Cu	Al						
6.45	1.6	6.31	6.89	0.59	–	–	20	80	60	2	2	[16]
7.18	1.49	5.68	4.29	1.96	1.78	–	20	80	60	2	2	[64]
21.8	3.2	4.6	2.7	0.03	1.2	1.1	10	80	–	100% excess	15	[65]
22.65	3.37	3.32	4.58	0.26	–	1.62	10	75	120	2	2	[66]
8.47	2.84	5.57	10.2	0.29	0.01	2.53	10	–	–	1.25	0.15 mol·L ⁻¹ Na ₂ S ₂ O ₅	[67]
4.606	2.931	0.0535	14.82	0.03125	0.516	–	–	–	–	3% (v/v)	0.3	[68]
19.20	4.68	6.46	14.14	1.13	0.36	1.01	10	70	120	2	10	[69]
21.506	3.376	5.44	7.491	0.413	0	0.682	7.5	–	–	1	–	[70]
34.663	12.26	21.955	40.67	–	–	–	–	–	–	–	–	[71]
8.4	2.8	6.8	7.4	0.1	4.3	2.2	10	50	60	2	3	This work
5.645	3.817	5.877	12.646	–	–	2.912	10	80	240	4	–	[72] ^a
11.4	5.3	11.7	12.2	–	–	–	10	60	–	2	5	[73] ^b
32.73	2.265	18.7	0.075	–	–	–	10	–	–	2	4	[19] ^b
11.32	1.76	11.51	9.18	–	–	–	8	90	120	4	2	[74] ^b
18.7	1.1	7.4	7.2	–	–	–	–	–	–	–	–	[75] ^c
8.11	7.23	8.32	6.23	0.23	0.21	–	–	–	–	–	–	[76] ^c
8	1.25	1	0.95	0.35	1	0.7	–	–	–	–	–	[77] ^c
24.79	6.68	5.91	6.24	0.27	0.0013	–	–	–	–	–	–	[78] ^d

(a) Pretreatment of the black mass before leaching, e.g., roasting; (b) pretreatment of the leachate, e.g., pH adjustment; (c) synthetic solution; (d) industrial solution; “–” not available

formation, while providing insights into the limitations of equilibrium-based models and the influence of kinetic effects in real systems. This integrated approach aims to contribute to the ongoing development of precipitation-based processes for LIB recycling, particularly in the context of producing solid products relevant to cathode precursor materials.

2 Methodology

Thermodynamic simulations were performed for the metal solutions mimicking the LIB leachate, using NaOH as the precipitant agent. The results were used in two different precipitation strategies: (1) FP and (2) SP, as observed in Fig. 1.

2.1 Thermodynamic simulation

OLI Studio Stream Analyzer (v11.5, OLI Systems, Inc.) was used to simulate solution speciation and metal-salt's precipitation. This study employed a synthetic multicomponent solution intended to simulate a simplified leachate from the recycling of LIBs. The focus was placed on the primary metal ions—Li⁺, Co²⁺, Ni²⁺, and Mn²⁺—to allow a clearer evaluation of the precipitation behavior and recovery process. The exclusion of impurities at this stage was intentional to reduce system complexity, with the understanding that their influence shall be addressed in future work as the methodology advances. Metal sulfates and sulfuric acid are added to the software in quantities to fulfil the mass balance to obtain the same ion composi-

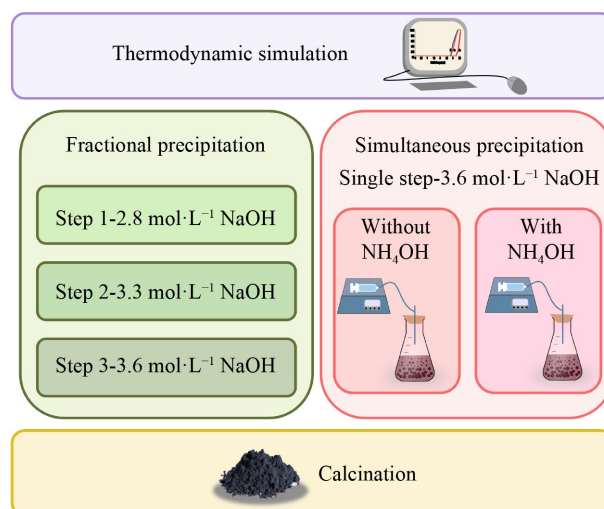


Fig. 1 Methodology workflow: thermodynamic simulation, simultaneous and fractional precipitation experiments, and calcination.

tions and concentrations in the solution. The input composition for the solution was: Li₂SO₄ 22.17 g·L⁻¹, CoSO₄ 22.09 g·L⁻¹, NiSO₄ 19.51 g·L⁻¹, MnSO₄ 18.69 g·L⁻¹, and 126.11 g·L⁻¹ of H₂SO₄. The mixed solvent electrolyte with the Soave-Redlich-Kwong model was the chosen framework [61]. Precipitation simulations were made for concentration ranges of NaOH from 0.1 to 4 mol·L⁻¹, without and with the presence of ammonium hydroxide (0.3 mol·L⁻¹ NH₄OH in solution), a typical solution added in the production of NMC precursors, as a chelating agent.

2.2 Synthetic solution preparation and precipitants

The solution was prepared by dissolving analytical-grade sulfate salts of Li, Co, Ni, and Mn in Milli-Q water (18.2 M Ω -cm at 25 °C), along with H₂SO₄. The specific chemical reagents and their concentrations are presented in Table 2. The NaOH solution used as the precipitating agent was prepared at a concentration of 144 g·L⁻¹ (1310-73-2, Merck). Substitute by: ammonium hydroxide 28%–30% (1336-21-6, J.T. Baker) was added before the precipitant agent in experiments to evaluate the impact of the presence of chelating agent in the solution.

2.3 Fractional precipitation

Based on the results from the thermodynamic simulations, FP experiment was designed with three steps defined for the addition of precipitant (pH-adjustment (D1), Co and Ni recovery (D2), and Mn recovery (D3)), represented respectively in blue, green, and red on Fig. 2. In each step, the precipitant was added using syringe pumps (New Era Pump Systems, Inc.) with a flow rate of 200 mL·h⁻¹, which ensured a thorough mixing regimen in

Table 2 Synthetic leachate stock solution composition

Chemical (CAS, Manufacturer)	Concentration
Lithium sulfate anhydrous (10377-48-7, Thermo Scientific)	22.17 g·L ⁻¹
Cobalt(II) sulfate heptahydrate (1026-24-1, Thermo Scientific)	40.06 g·L ⁻¹
Nickel(II) sulfate hexahydrate (10101-97-0, Sigma Aldrich)	33.16 g·L ⁻¹
Manganese(II) sulfate monohydrate (10034-96-5, VWR International)	20.93 g·L ⁻¹
H ₂ SO ₄ 95%–97% (7664-93-9, Merck)	75 mL·L ⁻¹

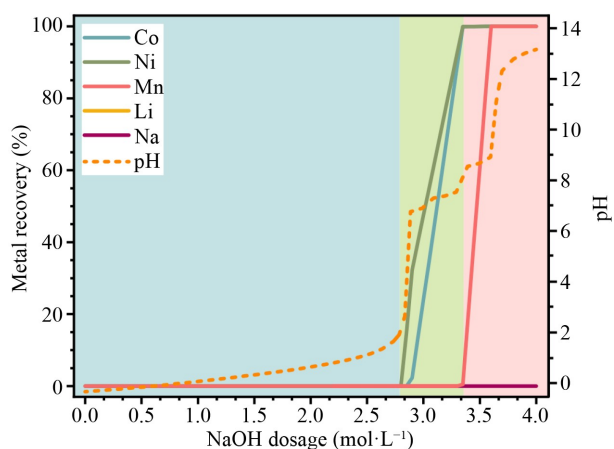


Fig. 2 Simulation of metal recovery from the multicomponent solution on OLI Stream Analyzer according to the added NaOH. Blue area represents the first step of fractional precipitation (D1) processes where no precipitation is seen, green area represents the second step of fractional precipitation (D2) where precipitation of Co and Ni are predicted, and red area represents the third step of fractional precipitation (D3) where precipitation of Mn is predicted.

the reactor using magnetic stirrer agitation. The resulting suspension was kept under stirring for 24 h at room temperature, with pH monitored (ORION STAR A211, Thermo Scientific). After, the solution was filtered using a vacuum filtration system and filter paper. The supernatant was recovered from the filtration and used in the subsequent step, where more precipitant was added. A liquid sample was retrieved and filtered with a 0.45 μ m syringe filter before dilution for analysis in the inductively coupled plasma optical emission spectrometer (ICP-OES, iCAP 7000 Series, Thermo Scientific) for residual metal content in the liquid. The recovered solid was washed by adding 90 mL MilliQ water and agitating for 30 s in the vortex (Vortex-Genie 2, Labor. A), followed by new filtration under vacuum. The solids were dried in the oven at 50 °C for at least 12 h before storage or further analysis.

2.4 Simultaneous precipitation

The SP experiments consisted of the single step addition of equal parts of the metal-containing solution and precipitant in the concentration referred to as the maximal recovery rate obtained in the simulations of 3.6 mol·L⁻¹ for NaOH, as shown in Fig. 2. The precipitant solution was added as described for fractional precipitation. A liquid sample was recovered for analysis while the filtered solid was washed and dried.

2.5 Calcination

Solids were calcinated in an oven (CARBOLITE CWF1200) under normal atmospheric conditions, adapting the procedure reported by He et al. [47]. Samples were loaded into ceramic cups, preheated at 100 °C for 1 h, then heated to 500 °C for 5 h and lastly heated to 900 °C for 12 h. The samples were characterized by powder X-ray diffraction (XRD, X'Pert Pro, PANalytical with Cu K α source) and scanning electron microscopy (SEM, S-3700N, Hitachi) coupled with energy-dispersive X-ray spectroscopy (EDS, Esprit 1.9 Quantax 400).

3 Results and discussion

3.1 Thermodynamic simulation

The results for the thermodynamic simulation are plotted as metal removal (%) and pH vs. NaOH dosage (mol·L⁻¹) (Fig. 2). The simulated conditions aimed to assess the solution's response to the addition of NaOH. This choice of compound is advantageous for industrial applications due to its availability as the preferential solution for pH adjustment in hydrometallurgical processes, cost-effectiveness, and high solubility (hence, sodium salts should

not be formed in this precipitation process) [1].

The process can be categorized into three primary stages. In the initial step (D1), represented by the blue area in Fig. 2, with NaOH concentrations below $2.8 \text{ mol}\cdot\text{L}^{-1}$, no solid precipitation is taking place. At the same time, the pH varies from -0.15 to 2.87 . This is proportional to the concentration of sulfuric acid present in the system, since the acid is being neutralized. The second step in the simulation (D2), colored in green (Fig. 2), entails the precipitation of Co and Ni. A noteworthy behavior of this system is the indissociable SP of Ni and Co hydroxides in this step, followed by manganese hydroxide fractional precipitation. Accordingly, approximately 92.7% of the Ni can be precipitated in the form of $\text{Ni}(\text{OH})_2$, and 89.2% of the cobalt precipitates as $\text{Co}(\text{OH})_2$ with the addition of $3.3 \text{ mol}\cdot\text{L}^{-1}$ NaOH. Thus, this step should yield a solid fraction containing only Co and Ni hydroxide. No stable cocrytals were found in the simulations. In the third step (D3), colored red in Fig. 2, when the precipitant concentration reaches $3.6 \text{ mol}\cdot\text{L}^{-1}$ the complete recovery of manganese ($\text{Mn}(\text{OH})_2$), along with the remaining Co (10.8%) and Ni (7.4%), is achieved. The solid is expected to be a mixture of Mn, Co, and Ni hydroxides as separate solid phases. No other phase with two or three metals in the same solid is indicated as stable in the simulation. No Li recovery is anticipated within this process due to the high solubility of the possible compounds (considering the ions present in solution: LiOH , Li_2SO_4).

The thermodynamic results show the possibility for fractional recovery of two different solid products: one containing only Co and Ni, representing most of these metals' recovery from the solution; and another comprised of mostly manganese and a smaller concentration of the remaining Co and Ni.

3.2 Fractional precipitation

Figure 3 shows the results for FP slightly as guided by the thermodynamic simulations. On the first reagent addition,

the NaOH concentration reached $2.8 \text{ mol}\cdot\text{L}^{-1}$. While the simulations showed no solid formation, a very fine solid was observed. The solution was filtered after 24 h, and some solid was retained in the paper, but insufficient to be characterized. The ICP-OES analysis of the remaining liquid (Fig. 3(a)) pointed to the removal of 16.9% of the manganese content from the initial solution, as well as 6.9% of Ni and 4.5% of Co, even though simulations predicted no precipitation at this stage. NaOH was initially added to the system to neutralize part of the acid content, reaching a pH of 3.1. The pH measured during the slow addition of precipitant (Fig. 3(b)) shows a good match with the simulation: a slow increase in pH occurred as sulfuric acid was neutralized followed by a rapid rise in pH, corresponding to the precipitation of $\text{Ni}(\text{OH})_2$ and $\text{Co}(\text{OH})_2$ in the simulation. As $\text{Mn}(\text{OH})_2$ began to precipitate, the curve exhibited a shift in slope. It is noteworthy that the equilibrium pH plays a critical role in determining the efficiency and selectivity of the precipitation in such complex systems. In this study, pH was monitored continuously during NaOH addition, but the measured values, although relatively well matching with the simulations, may not reflect equilibrium conditions due to ongoing reaction kinetics and mixing dynamics. As shown in Fig. 3(b), experimental pH values were mostly higher than simulated ones at equivalent NaOH dosages, which likely contributed to the observed deviations in metal recovery—particularly the unexpected recoveries in the first step (D1). This discrepancy highlights the fact that NaOH dosage alone is not a reliable alternative for equilibrium pH control, especially in complex multicomponent systems. While controlling the process via dosage was experimentally more feasible for this study, future work—particularly with real LIB leachates—shall incorporate equilibrium pH measurements.

D2 (Fig. 3(a)) shows the highest removal rates for Ni and Co, with respectively 89.7% and 76.8% recovery, inferior to the simulation predictions (92.7% for Ni and 89.2% for Co). Mn and Li were also recovered in this

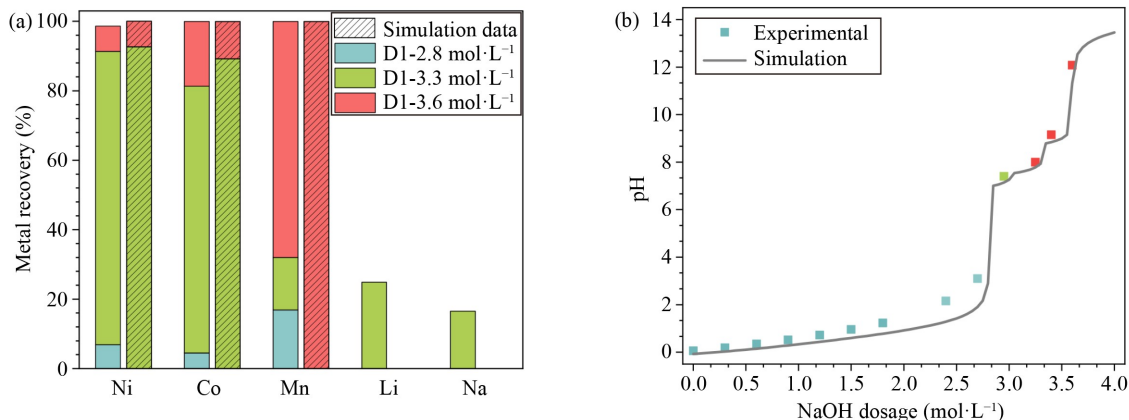


Fig. 3 Fractional experiment: (a) metal recovery and (b) pH monitoring through the precipitant addition (error bars were not plotted as they were not visible enough. Error on Li D2 is 4.5% and Mn D2 is 1.37%; all other data points have an error of less than 1%).

step, with Li reaching 24.9% removal and Mn reaching 15.1%. Na removal was also observed (around 16%). These results show a discrepancy when compared to the simulations and existing literature concerning the removal of Li and Na from the solution. From the thermodynamic simulation perspective, considering that equilibrium is reached, the observed discrepancies are likely attributed to factors unaccounted for, e.g., kinetics, fluid inclusions, and surface adsorption phenomena. Furthermore, the software seemingly lacks complex compounds such as $\text{Co}_x\text{Ni}_y\text{Mn}_{1-x-y}(\text{OH})_2$ in its database, thus assuming the formation of single metal hydroxides, rather than the mixed hydroxide phase. In addition, the literature on similar materials derived from LIB recycling leachates rarely mentions the contamination of the solid phase with Li and Na [79] ions, as was observed in our study. This discrepancy suggests a potential link between the amorphous character of the produced materials and the impurity retention, which needs to be further investigated.

Both pH and concentration achieved during the process are lower than the necessary levels for lithium hydroxide precipitation [80]. Additionally, the solubility of Na_2SO_4 , which is reported to be 28.2 g per 100 g of water at 25 °C [81], has not been reached in our solution (14.4 g/100 g_{water}). Thus, the conditions under which the experiments were conducted did not favor the formation of any Na or Li solid. Although Li and Na solubility limits were not exceeded, their removal in D2 may be caused by kinetic effects, coprecipitation (not captured by the simulation), and/or surface adsorption. We speculate that the rapid formation of amorphous solids in D2 could have led to the entrapment of mother liquor in the solid matrix and enhanced ion adsorption. At the same time, in D3, slightly slower (and lower-yielding) precipitation takes place, due to lower supersaturation (since most metals have already precipitated in D2), which may have limited these effects. The third reagent addition (D3) shows the removal of the remaining Mn, alongside Co and Ni, as predicted, yet in different proportions: 64.3%, 18.7%, and

7.3%, respectively.

The products of D2 and D3 were analyzed on XRD, which revealed an amorphous solid (Fig. A1, cf. Electronic Supplementary Material (ESM), section A), from which no conclusive results could be extracted from the diffraction patterns. Hence, the solids were calcined before further analysis, presented in Fig. 4. XRD analysis was conducted to identify the phases present in the calcinated solids. After the calcination, the diffractograms were analyzed, and no definite matches were found for possible oxides derived from the initial hydroxides, likely due to solid-state reactions taking place at high temperature. Partial matches were found with $\text{Mn}_{0.25}\text{Ni}_{0.75}\text{O}$ [82] and $\text{Li}_{11.92}\text{Mn}_{11.12}\text{O}_{32.0}$ [83] as observed in Fig. B1 (cf. ESM, section B). Nevertheless, sample D2 showed several peaks that aligned with those of a material produced by Yang et al. [84]—a mixed NMC hydroxide. In their study, the material was synthesized in a controlled reactor using an NH_4OH inflow and temperature regulation to produce $\text{Ni}_x\text{Co}_y\text{Mn}_{1-x-y}(\text{OH})_2$, which, through lithiation later yielded spherical $\text{LiNi}_x\text{Co}_y\text{Mn}_{1-x-y}\text{O}_2$ particles [84]. However, additional peaks indicated the presence of a second phase, to which no clear match could be found. D3 shows peaks pointing to the formation of the same compound, despite very different proportions of Co, Ni, and Mn, compared to D2.

Figure 5 shows SEM-EDS results from the solid recovered in D2 after calcination. Calcined solids show very uniform morphology with very small particles and few discrepant larger particles. As observed in Fig. 5(a), two different phases appear in the backscattered electrons (BSE) image (indicated by the different shades of gray), corroborating the XRD results (unmatched peaks). EDS reveals that the discrepant phases contain sodium and sulfur, indicating the possible formation of a sodium phase. When zoomed in, an unusual solid morphology was found, with regular shape, with 5 sides, and hollowed faces of the crystal, with tiny crystallites agglomerated on some parts comprising a different solid phase, as

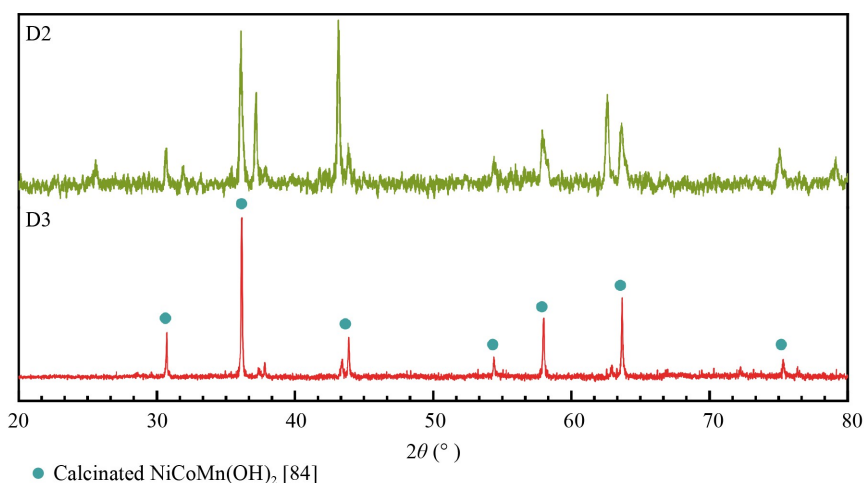


Fig. 4 XRD characterization of solids D2 and D3 after calcination.

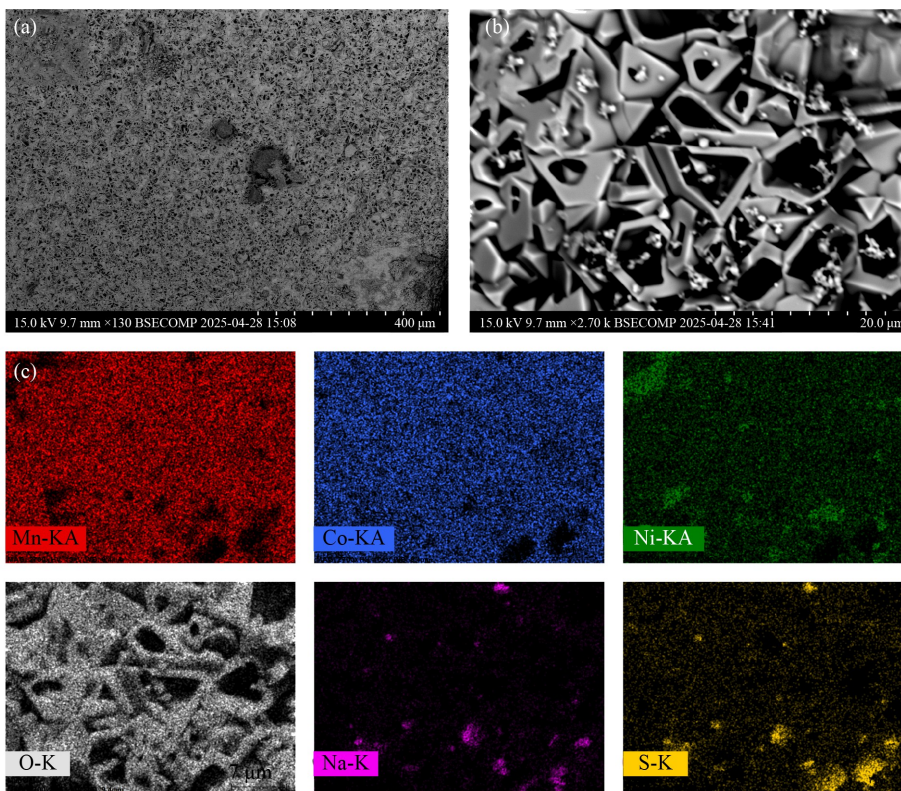


Fig. 5 Image characterization of solid D2 after calcination: (a) BSE image from SEM amplification $\times 130$, and (b) BSE image from SEM amplification $\times 1.7$ K; (c) EDS elemental mapping.

presented in Figs. 5(b) and 5(d). Figure 5(c) shows the EDS elemental mapping. It revealed the crystallites to be rich in Na and S—which does not match the unidentified XRD peaks—while the rest of the sample surface was comprised of Co, Ni, and Mn uniformly distributed. This points to the formation of mixed transition metal oxides after calcination at 900 °C. EDS could not be used to detect lithium, due to a limitation of the sensitivity of the equipment in the detection of very low-energy X-rays preventing the measurement of elements lighter than boron in the periodic Table [85,86].

The solid recovered in the final step of fractional precipitation (D3) consists of agglomerates of very tiny (in the order of nm) crystals as observed in Fig. C1 (cf. ESM, section C). A secondary phase containing Na and S is also present. Even though the Na removal in this step was not detected via ICP-OES, traces of it remained in the solid, likely due to drying of the remaining solution adhered to the solid, suggesting that a more rigorous washing procedure may be necessary to reduce or prevent this contamination. These observations are consistent with ICP analysis and the thermodynamic simulations for step 3 (Fig. 3(a)), which indicated the removal of Mn along with lower amounts of Co and Ni.

The amorphous characteristic of the product prevented the confirmation of the initial solid product as the predicted hydroxides. Nevertheless, the results from SEM-EDS of the calcined samples along with the ICP-OES of the remaining solution show that the fractional

precipitation was not successful in achieving the separate fractions of Co/Ni (D2) and rich in Mn (D3), as per the simulations, i.e., the partial precipitation of metals showed low selectivity and did not yield a material with the desired composition or purity. This discrepancy suggests that the kinetics plays a larger role in the precipitation from multicomponent solutions, deeming simulations in equilibrium less accurate. It is also possible that the formation of solid phases not predicted by thermodynamic models happened, highlighting the need for further research into multicomponent crystallization systems. Moreover, the unexpected presence of Na and the concomitant recovery of Li indicate that phenomena other than just precipitation may be taking place in the process, such as adsorption of the Li and Na ions on the amorphous materials or other impurity incorporation mechanisms such as fluid inclusions, or isomorphic substitution [84,85].

3.3 Simultaneous Precipitation

SP was initially envisioned as a process capable of yielding a solid comprising three distinct populations, each containing one of the transition metals in separate phases, as predicted by thermodynamic simulations. However, the results obtained from FP experiments indicated that those phases were probably not formed, and the best match found under those conditions was likely a mixed hydroxide ($\text{Ni}_x\text{Co}_y\text{Mn}_{1-x-y}(\text{OH})_2$) [84]. Such material can

be used as an NMC precursor for the manufacturing of battery cathodes [41,85]. The similarity of the FP solid with the NMC precursor highlights the potential of SP to recover multiple transition metals in a single step—even in the presence of Li in solution and absence of typical requirements for NMC precursor synthesis, such as the use of NH_4OH as a chelating agent or an inert atmosphere. According to Malik et al. [29], the most typical coprecipitation to produce NMC cathode starts with the precipitation of Co, Ni, and Mn hydroxides from a solution made of these metal sulfates in water, where NH_4OH is added as a chelating agent and NaOH is used as a precipitant. Therefore, the SP experiments were performed without and with the addition of ammonium hydroxide, in line with standard protocols for producing battery-grade NMC precursors. The concentration of ammonium ions ($0.3 \text{ mol}\cdot\text{L}^{-1}$) was selected based on findings from Yang et al. [84], where the range of 0.15 to $0.43 \text{ mol}\cdot\text{L}^{-1}$ NH_4OH yielded optimal results for the formation of mixed hydroxides. Washing of the crystals was performed twice to minimize the presence of impurities.

For the initial experiment, using only NaOH as the precipitating agent, ICP-OES analysis of the residual solution confirmed nearly complete recovery of Co, Ni, and Mn ($> 99.7\%$), along with partial removal of Li and Na with 15.6% and 9.8% respectively, as shown in Fig. 6(a). The pH profile recorded during the gradual addition of NaOH (Fig. 6(b)) aligned well with the simulation results.

The SP experiment using ammonium hydroxide was conducted to evaluate metal recovery and the morphology of the resulting material, providing a basis for comparison with the materials produced using the precipitation strategy proposed in this study. According to literature, added to Co-Ni-Mn solutions, ammonium hydroxide acts as a chelating agent, responsible for assuring the precipitation of $\text{NiMnCo}_x\text{OH}_y$, other than single metal hydroxides. Its role in the solution is also associated by

some authors with particle size morphology (spherically shaped particles) and uniformity, while lowering the sulfate impurities in the final product, which in its turn aids the electrochemical characteristics of the precursors [87–89]. As shown in Fig. 6(a), the overall metal recovery performance in the presence of ammonium was closer to the main process, including Li, other than the lower metal recovery foreseen by the thermodynamic simulation of the system NaOH + NH_4OH . However, the removal of Na ions was expressively reduced under these conditions, in a closer match to the simulation where mirabilite ($\text{Na}_2\text{SO}_4\cdot 10\text{H}_2\text{O}$) is foreseen to form in the presence of NaOH in concentrations over $3.3 \text{ mol}\cdot\text{L}^{-1}$.

To investigate the unexpected Li behavior, kinetic experiments were conducted. Figure D1 (cf. ESM, section D) shows that Li removal occurred rapidly within the first 5 min after precipitant addition, with concentrations stabilizing after 24 h, despite some fluctuations in the first hour. For the transition metals, the complete recovery happened in the first 5 min, yielding results aligned with thermodynamic predictions. The rapid kinetics observed are likely driven by the high supersaturation induced by the addition of the precipitant, which in turn promotes fast nucleation and the formation of amorphous phases and agglomerates [86,90]. This supports the hypothesis that Li may be physically trapped within fluid inclusions or adsorbed onto the surfaces of amorphous solids, rather than precipitating as a distinct phase. Moreover, the gradual co-removal of Li and Na suggests that extended residence times may be detrimental to Li recovery, as Li is intended to be precipitated separately in a later step using a different reagent. This contrasts with standard processes for synthesizing NMC precursors, where residence time plays a key role in particle aging and crystallinity but typically involves only Ni, Mn, and Co—without considering Li incorporation. In our study, solid samples aged for 1, 7, and 14 days showed no significant improvements in crystallinity based on XRD analysis (cf. ESM), further supporting the limited benefit

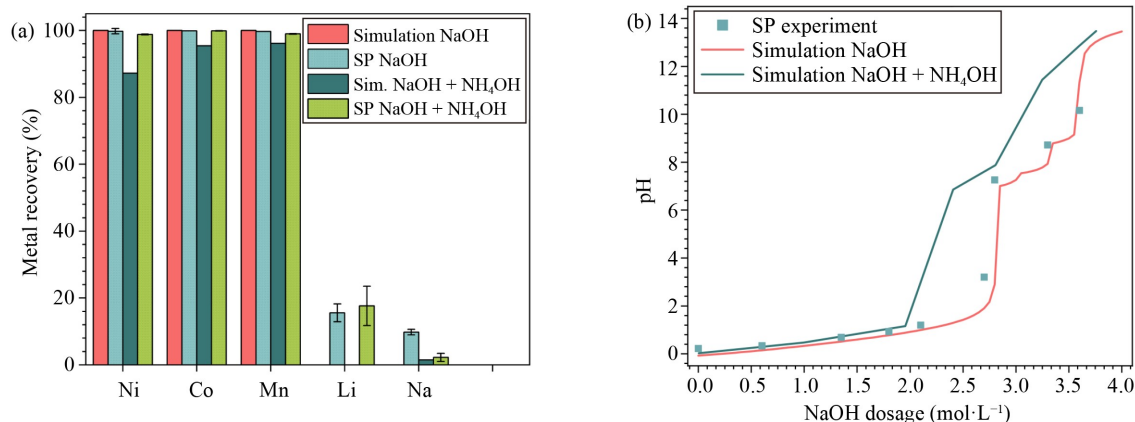


Fig. 6 SP of hydroxides. (a) Simulation and experimental metal recovery for a dosage of $3.6 \text{ mol}\cdot\text{L}^{-1}$ NaOH with and without NH_4OH addition. (b) pH measurements through precipitant addition and thermodynamic simulation of pH variation through NaOH and NaOH + NH_4OH addition.

of prolonged aging in this context.

Figure 7 shows the XRD analysis for the calcined solids from SP without and with ammonium addition. The diffractogram shows that, despite the chelating agent, the solids formed in the two experiments were very similar, and coincided with the NMC phase found in literature [84]. No formation of a specific sodium phase of mirabilite ($\text{Na}_2\text{SO}_4 \cdot 10\text{H}_2\text{O}$), nor thernadite (Na_2SO_4 , its dehydrated form [91]), as foreseen in thermodynamic simulations, could be observed in the spectrogram before and after calcination.

SEM images revealed that the SP product is highly agglomerated and porous (Figs. 8(a) and 8(b)). EDS shows no presence of Na and S in the sample, with BSE images confirming the presence of a single-phase solid where the different metals can be seen uniformly dispersed (Fig. 8(c)), highlighting that a thorough washing protocol can remove impurities from the solids.

Nonetheless, the presence of sodium (from SEM

analysis) and the recovery of Li from the ICP-OES analysis were shown to be somewhat different from the desirable for an NMC precursor. Li is usually only added to the mix of the NMC precursor before the calcination step [41,47], while Na is considered an undesired impurity [71,79]. Sodium-ion batteries are being studied, reaching similar properties to LIBs [92,93], indicating the possibility of a mixed battery containing both cations in the future [79]. Li and Na impact on the solid material performance as a cathode material needs to be further investigated.

An attempt was made to remove Li and Na from the solid. The recovered material was washed in three steps—W1, W2, and W3—with solid samples being recovered from each step and the liquid analyzed in the ICP-OES. The results were used to estimate the metal removal from the solids, in each wash step as plotted in Fig. E1 (cf. ESM, section E). Three steps of washing with abundant water at room temperature were shown to

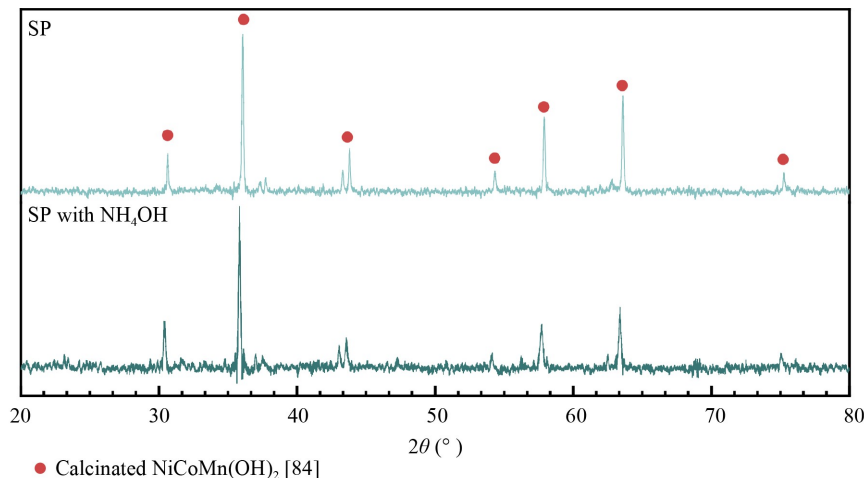


Fig. 7 XRD characterization of solids of SP and SP with NH_4OH after calcination (SP with NH_4OH).

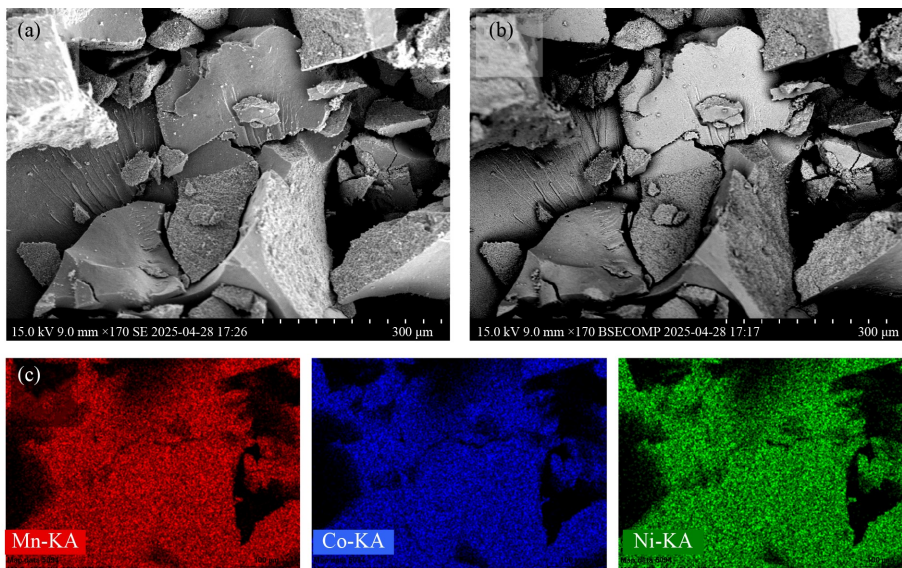


Fig. 8 SEM images: (a) BSE and (b) SE of calcined SP sample, double washed; (c) chemical mapping.

reduce undesirable metals from the solid, without washing out the target material. The removal of transition metals, Co, Ni, and Mn, is minimal due to their low solubility in water, reaching respective concentrations of 0.05%, 0.03%, and 0.09% in total. Li and Na total removal reached 21.6%, with W1 and W2 responsible for 9% and 9.5% of the removal.

For the ammonium experiment, SEM-EDS analysis revealed a similar solid product (Figs. 9(a) and 9(b)). Both samples show a uniform dispersion of Co, Ni, and Mn throughout the solid, evidencing the formation of the mixed oxides after the calcination. However, Na and S were observed in specific areas of the solid from the experiment with ammonium hydroxide (Fig. 9(c)), suggesting the formation of Na salts (mirabilite or thernadite) as foreseen in the thermodynamic simulation. The presence of impurities—particularly Na and S—is responsible for hindering the formation of well-ordered layered structures in the material, consequently reducing the material's crystallinity and particle size. Na was classified as a medium impurity with concentrations between 50 and 1000 mg·L⁻¹ in the precursor obtained from LIB leachates [71,90].

The results suggest that SP may be suitable for producing NMC precursor materials directly from sulfuric acid LIB leachates, provided that a washing protocol is optimized to reduce the level of impurities in the sample. However, further experiments characterizing

the material's physicochemical properties are required, as well as SP with real LIB leachates. These analyses should be compared against commercial NMC materials to assess the quality, performance potential, and suitability of the synthesized product as a battery precursor.

The discrepancies between simulation and experimental results may be attributed to several factors not accounted for in the thermodynamic simulations. These include the kinetics of precipitation, and the effects of local supersaturation levels, which can significantly influence metal recovery. Additionally, the formation of complex salts—containing more than one of the metals—was not predicted, also contributing to these discrepancies. Furthermore, there is a tendency for the material to form amorphous structures rather than well-defined crystals before calcination. This observation highlights the need for further understanding of these amorphous phases and their implications for material properties. The remaining solution recovered from the process is still rich in Na, Li, and sulphates. Lithium recovery potential needs to be further explored. Possible routes can be through lithium carbonate, lithium hydroxide, or lithium sulfate crystallization [94,95].

4 Conclusions

This study investigated the FP and SP of transition metals

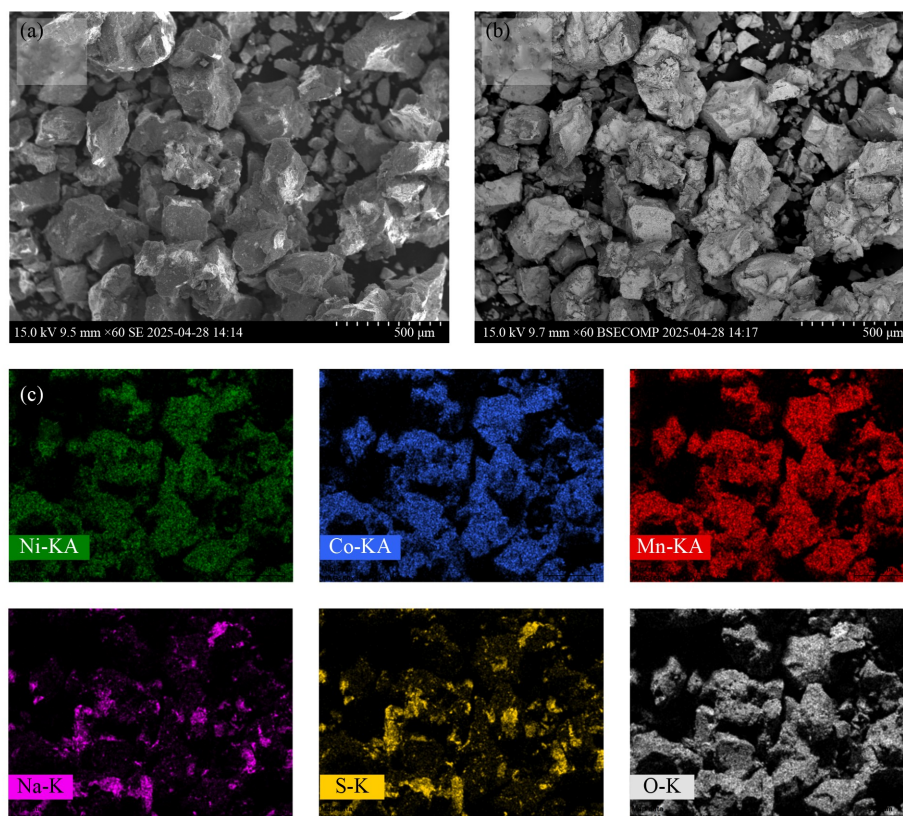


Fig. 9 SEM images from experiment SP in the presence of NH₄OH, (a) SE, (b) BSE, and (c) chemical mapping.

from a synthetic solution containing the main metals found in common LIB leachate in a similar concentration of sulfuric acid. FP was found ineffective for separating Ni, Co, and Mn. Although the D2 contains primarily Co (76.8%) and Ni (89.7%), the presence of Mn (15%), Li (25%), and Na in the solid was still observed. D3 showed enhanced Mn removal (68%), the value is below expected in simulations, and was accompanied by significant levels of Co (18.7%) and Ni (7.3%). As a result, the process produced a mixed hydroxide phase, which deviated from the expected thermodynamic outcomes. While fractional precipitation was found to be impractical for selective recovery, the formation of a Co-Ni-Mn mixed hydroxide aligns with the composition of NMC precursors, offering potential value for future applications. The co-precipitation of lithium and sodium reveals the strong influence of kinetics, and possibly impurity adsorption in the amorphous material, which could not be estimated by simulations. The presence of sodium and sulfur led to the observation of separate phases on the SEM-EDS analysis. This calls for deeper studies on the mechanisms of impurity incorporation.

The application of a single precipitation step with and without the addition of ammonium hydroxide as a chelating agent both resulted in a recovery rate for Co, Ni, and Mn superior to 99.7%, together with 17.7% and 15.6% of Li, respectively. It produced a mixed hydroxide material, with SEM-EDS confirming consistent surface distribution of the transition metals. The overall performance of SP hints at a simpler and viable alternative for cathode precursor production, despite the presence of Li ions in the solution. It is noteworthy that results are specific to the simplified studied system and cannot yet be generalized to all LIB chemistries. Nonetheless, SP presents a promising alternative for multi-metal recovery from LIB leachates, supporting the development of more sustainable battery recycling processes and a circular economy around batteries. Future work will explore real leachates, impurity effects, and broader battery chemistries.

Competing interests The authors declare that they have no competing interests.

Electronic Supplementary Material Supplementary material is available in the online version of this article at <https://doi.org/10.1007/s11705-025-2610-x> and is accessible for authorized users.

Funding Note Open access funding provided by Royal Institute of Technology.

Open Access This article is licensed under a Creative Commons Attribution 4.0 International License, which permits use, sharing, adaptation, distribution and reproduction in any medium or format, as long as you give appropriate credit to the original author(s) and the source, provide a link to the Creative Commons licence, and indicate if changes were made. The images or other third party material in this article are included in the article's Creative Commons licence, unless indicated otherwise in a credit

line to the material. If material is not included in the article's Creative Commons licence and your intended use is not permitted by statutory regulation or exceeds the permitted use, you will need to obtain permission directly from the copyright holder. To view a copy of this licence, visit <https://creativecommons.org/licenses/by/4.0/>.

References

1. Neumann J, Petranikova M, Meeus M, Gamarra J D, Younesi R, Winter M, Nowak S. Recycling of lithium-ion batteries—current state of the art, circular economy, and next generation recycling. *Advanced Energy Materials*, 2022, 12(17): 2102917–2102926
2. Grohol M, Veeh C. Study on the critical raw materials for the EU 2023: final report. Publications Office of the European Union, 2023
3. Xiao J, Niu B, Lu J, Hong J, Zhou T, Xu Z. Perspective on recycling technologies for critical metals from spent lithium-ion batteries. *Chemical Engineering Journal*, 2024, 496: 154338
4. Zhou B, Su H, Liu W, Zhu Z, Wang L, Qi T. Solvent extraction of metal ions from the leaching solutions of waste lithium-ion battery materials: a review. *Separation and Purification Technology*, 2025, 354: 129173
5. Lei S, Sun W, Yang Y. Solvent extraction for recycling of spent lithium-ion batteries. *Journal of Hazardous Materials*, 2022, 424: 127654
6. Costa C M, Barbosa J C, Gonçalves R, Castro H, Campo F J D, Lanceros-Méndez S. Recycling and environmental issues of lithium-ion batteries: advances, challenges, and opportunities. *Energy Storage Materials*, 2021, 37: 433–465
7. Yang Y, Okonkwo E G, Huang G, Xu S, Sun W, He Y. On the sustainability of lithium ion battery industry—a review and perspective. *Energy Storage Materials*, 2021, 36: 186–212
8. Zhang Y, Hu Y, Wang L, Sun W. Systematic review of lithium extraction from salt-lake brines via precipitation approaches. *Minerals Engineering*, 2019, 139: 105868
9. Nicol M, Welham N, Senanayake G. Precipitation and crystallization. *Hydrometallurgy*, 2022, 2: 84–115
10. Barik S P, Prabakaran G, Kumar L. Leaching and separation of Co and Mn from electrode materials of spent lithium-ion batteries using hydrochloric acid: laboratory and pilot scale study. *Journal of Cleaner Production*, 2017, 147: 37–43
11. Granata G, Moscardini E, Pagnanelli F, Trabucco F, Toro L. Product recovery from Li-ion battery wastes coming from an industrial pre-treatment plant: lab scale tests and process simulations. *Journal of Power Sources*, 2012, 206: 393–401
12. Nayaka G P, Manjanna J, Pai K V, Vadavi R, Keny S J, Tripathi V S. Recovery of valuable metal ions from the spent lithium-ion battery using aqueous mixture of mild organic acids as alternative to mineral acids. *Hydrometallurgy*, 2015, 151: 73–77
13. Chen L, Tang X, Zhang Y, Li L, Zeng Z, Zhang Y. Process for the recovery of cobalt oxalate from spent lithium-ion batteries. *Hydrometallurgy*, 2011, 108(1-2): 80–86
14. Meshram P, Pandey B D, Mankhand T R. Hydrometallurgical processing of spent lithium ion batteries (LIBs) in the presence of a reducing agent with emphasis on kinetics of leaching. *Chemical*

- Engineering Journal, 2015, 281: 418–427
15. Zhu S G, He W Z, Li G M, Zhou X, Zhang X J, Huang J W. Recovery of Co and Li from spent lithium-ion batteries by combination method of acid leaching and chemical precipitation. *Transactions of Nonferrous Metals Society of China*, 2012, 22(9): 2274–2281
 16. Chen X, Chen Y, Zhou T, Liu D, Hu H, Fan S. Hydrometallurgical recovery of metal values from sulfuric acid leaching liquor of spent lithium-ion batteries. *Waste Management*, 2015, 38: 349–356
 17. Chen X, Ma H, Luo C, Zhou T. Recovery of valuable metals from waste cathode materials of spent lithium-ion batteries using mild phosphoric acid. *Journal of Hazardous Materials*, 2017, 326: 77–86
 18. Wang R C, Lin Y C, Wu S H. A novel recovery process of metal values from the cathode active materials of the lithium-ion secondary batteries. *Hydrometallurgy*, 2009, 99(3): 194–201
 19. Nayl A A, Elkhashab R A, Badawy S M, El-Khateeb M A. Acid leaching of mixed spent Li-ion batteries. *Arabian Journal of Chemistry*, 2017, 10: S3632–S3639
 20. Joulié M, Laucoumet R, Billy E. Hydrometallurgical process for the recovery of high value metals from spent lithium nickel cobalt aluminum oxide based lithium-ion batteries. *Journal of Power Sources*, 2014, 247: 551–555
 21. Asadi Dalini E, Karimi G, Zandevakili S. Treatment of valuable metals from leaching solution of spent lithium-ion batteries. *Minerals Engineering*, 2021, 173: 107226
 22. Wang H, Friedrich B. Development of a highly efficient hydrometallurgical recycling process for automotive Li-ion batteries. *Journal of Sustainable Metallurgy*, 2015, 1(2): 168–178
 23. Yi W T, Yan C Y, Ma P H. Crystallization kinetics of Li_2CO_3 from LiHCO_3 solutions. *Journal of Crystal Growth*, 2010, 312(16): 2345–2350
 24. Yao Y, Zhu M, Zhao Z, Tong B, Fan Y, Hua Z. Hydrometallurgical processes for recycling spent lithium-ion batteries: a critical review. *ACS Sustainable Chemistry & Engineering*, 2018, 6(11): 13611–13627
 25. Lv W, Wang Z, Cao H, Sun Y, Zhang Y, Sun Z. A critical review and analysis on the recycling of spent lithium-ion batteries. *ACS Sustainable Chemistry & Engineering*, 2018, 6(2): 1504–1521
 26. Shi P, Yang S, Wu G, Chen H, Chang D, Jie Y, Fang G, Mo C, Chen Y. Efficient separation and recovery of lithium and manganese from spent lithium-ion batteries powder leaching solution. *Separation and Purification Technology*, 2023, 309: 123063
 27. Xiao C, Zeng L. Thermodynamic study on recovery of lithium using phosphate precipitation method. *Hydrometallurgy*, 2018, 178: 283–286
 28. Velázquez-Martínez O, Valio J, Santasalo-Aarnio A, Reuter M, Serna-Guerrero R. A critical review of lithium-ion battery recycling processes from a circular economy perspective. *Batteries*, 2019, 5(4): 68
 29. Malik M, Chan K H, Azimi G. Review on the synthesis of $\text{LiNi}_x\text{Mn}_y\text{Co}_{1-x-y}\text{O}_2$ (NMC) cathodes for lithium-ion batteries. *Materials Today Energy*, 2022, 28: 101066
 30. Wang Z, Yang L, Xu C, Cheng J, Zhao J, Huang Q, Yang C. Advances in reactive co-precipitation technology for preparing high-performance cathodes. *Green Carbon*, 2023, 1(2): 193–209
 31. Yu L, Liu X, Feng S, Jia S, Zhang Y, Zhu J, Tang W, Wang J, Gong J. Recent progress on sustainable recycling of spent lithium-ion battery: efficient and closed-loop regeneration strategies for high-capacity layered NCM cathode materials. *Chemical Engineering Journal*, 2023, 476: 146733
 32. Rostami H, Valio J, Suominen P, Tynjälä P, Lassi U. Advancements in cathode technology, recycling strategies, and market dynamics: a comprehensive review of sodium ion batteries. *Chemical Engineering Journal*, 2024, 495: 153471
 33. Muzayanha S U, Yudha C S, Nur A, Widiyandari H, Haerudin H, Nilasary H, Fathoni F, Purwanto A. A fast metals recovery method for the synthesis of lithium nickel cobalt aluminum oxide material from cathode waste. *Metals*, 2019, 9(5): 615
 34. Fang J, Ding Z, Ling Y, Li J, Zhuge X, Luo Z, Ren Y, Luo K. Green recycling and regeneration of $\text{LiNi}_{0.5}\text{Co}_{0.2}\text{Mn}_{0.3}\text{O}_2$ from spent lithium-ion batteries assisted by sodium sulfate electrolysis. *Chemical Engineering Journal*, 2022, 440: 135880
 35. Tynjälä P, Laine P, Välikangas J, Kauppinen T, Lassi U. Effect of reaction conditions on the coprecipitation of $\text{Ni}(\text{OH})_2$ for lithium-ion batteries. *Chemical Engineering & Technology*, 2023, 46(11): 2279–2284
 36. Widiyandari H, Sukmawati A N, Sutanto H, Yudha C, Purwanto A. Synthesis of $\text{LiNi}_{0.8}\text{Mn}_{0.1}\text{Co}_{0.1}\text{O}_2$ cathode material by hydrothermal method for high energy density lithium ion battery. *Journal of Physics: Conference Series*, 2019, 1153: 012074
 37. Jumari A, Stulasti K N R, Halimah R N, Purwanto A, Aini L A, Mintarsih R. Production of $\text{LiNi}_{0.6}\text{Mn}_{0.2}\text{Co}_{0.2}\text{O}_2$ via fast oxalate precipitation for Li-ion. *AIP Conference Proceedings*, 2020, 2217(1): 030011
 38. Yudha C S, Hasanah L M, Muzayanha S U, Widiyandari H, Purwanto A. Synthesis and characterization of material $\text{LiNi}_{0.8}\text{Co}_{0.15}\text{Al}_{0.05}\text{O}_2$ using one-step Co-precipitation method for Li-ion batteries. *Jurnal Kimia Dan Pendidikan Kimia*, 2019, 4(3): 134
 39. Nurohmah A R, Ayuningtyas M, Yudha C S, Purwanto A, Widiyandari H. Synthesis and characterization of NMC622 cathode material modified by various cheap and abundant transition metals for Li-ion batteries. *Evergreen*, 2022, 9(2): 427–437
 40. Wijareni A S, Widiyandari H, Purwanto A, Arif A F, Mubarak M Z. Morphology and particle size of a synthesized NMC 811 cathode precursor with mixed hydroxide precipitate and nickel sulfate as nickel sources and comparison of their electrochemical performances in an NMC 811 lithium-ion battery. *Energies*, 2022, 15(16): 5794
 41. Berk R B, Beierling T, Metzger L, Gasteiger H A. Investigation of the particle formation mechanism during coprecipitation of Ni-rich hydroxide precursor for Li-ion cathode active material. *Journal of the Electrochemical Society*, 2023, 170(11): 110513
 42. Xu Z P, Zeng H C. Interconversion of brucite-like and hydrotalcite-like phases in cobalt hydroxide compounds. *Chemistry of Materials*, 1999, 11(1): 67–74
 43. Jo M, Ku H, Park S, Song J, Kwon K. Effects of residual lithium in the precursors of $\text{Li}[\text{Ni}_{1/3}\text{Co}_{1/3}\text{Mn}_{1/3}\text{O}_2]$ on their lithium-ion

- battery performance. *Journal of Physics and Chemistry of Solids*, 2018, 118: 47–52
44. Sa Q, Gratz E, He M, Lu W, Apelian D, Wang Y. Synthesis of high performance $\text{LiNi}_{1/3}\text{Mn}_{1/3}\text{Co}_{1/3}\text{O}_2$ from lithium ion battery recovery stream. *Journal of Power Sources*, 2015, 282: 140–145
 45. Qi Y, Wang M, Yuan L, Chen X. Closed-loop recycling of valuable metals from spent LiCoO_2 batteries through phosphate-chemistry-based process. *Chemical Engineering Journal*, 2023, 466: 143030
 46. Liu S, Yang J, Hao S, Jiang S, Li X, Dolotko O, Wu F, Li Y, He Z. Paving the way for electrochemical recycling of spent lithium-ion batteries: targeting the direct regeneration of de-lithiated materials. *Chemical Engineering Journal*, 2024, 479: 147607
 47. He L P, Sun S Y, Yu J G. Performance of $\text{LiNi}_{1/3}\text{Co}_{1/3}\text{Mn}_{1/3}\text{O}_2$ prepared from spent lithium-ion batteries by a carbonate coprecipitation method. *Ceramics International*, 2018, 44(1): 351–357
 48. Mersmann A. *Crystallization Technology Handbook*. Boca Raton: CRC Press, 2001
 49. Penha F M, Zago G P, Seckler M M. Strategies to control product characteristics in simultaneous crystallization of NaCl and KCl from aqueous solution: seeding with NaCl and KCl. *CrystEngComm*, 2020, 22(44): 7590–7600
 50. Liu W, Xu H, Shi X, Yang X. Fractional crystallization for extracting lithium from Cha'erhan tail brine. *Hydrometallurgy*, 2017, 167: 124–128
 51. Duman B Ö, Can İ B. Effects of staged-addition of acid on high Ni-Co recovery and low scale formation in HPAL of a lateritic ore. *Hydrometallurgy*, 2022, 213: 105935
 52. Guzhov B, Cassayre L, Barnabé A, Coppey N, Biscans B. Selective precipitation of rare earth double sulfate salts from industrial Ni-MH battery leachates: impact of downstream processing on product quality. *Batteries*, 2023, 9(12): 574
 53. Masindi V, Ndiritu J G, Maree J P. Fractional and step-wise recovery of chemical species from acid mine drainage using calcined cryptocrystalline magnesite nano-sheets: an experimental and geochemical modelling approach. *Journal of Environmental Chemical Engineering*, 2018, 6(2): 1634–1650
 54. Masmoudi-Soussi A, Hammas-Nasri I, Horchani-Naifer K, Férid M. Rare earths recovery by fractional precipitation from a sulfuric leach liquor obtained after phosphogypsum processing. *Hydrometallurgy*, 2020, 191: 105253
 55. Shu J, Wu H, Chen M, Peng H, Li B, Liu R, Liu Z, Wang B, Huang Y, Hu Z. Fractional removal of manganese and ammonia nitrogen from electrolytic metal manganese residue leachate using carbonate and struvite precipitation. *Water Research*, 2019, 153: 229–238
 56. Chen T, Lei C, Yan B, Xiao X. Metal recovery from the copper sulfide tailing with leaching and fractional precipitation technology. *Hydrometallurgy*, 2014, 147–148: 178–182
 57. Meenan P A, Anderson S R, Klug D L. The influence of impurities and solvents on crystallization. *Handbook of Industrial Crystallization*. Amsterdam: Elsevier, 2002, 67–100
 58. de Vasconcellos M E, Queiroz C A D S, Abrão A. Sequential separation of the yttrium—heavy rare earths by fractional hydroxide precipitation. *Journal of Alloys and Compounds*, 2004, 374(1–2): 405–407
 59. Clarkson A I, Bogle I D L, Titchener-Hooker N J. Modelling and simulation of fractional precipitation—comparison with pilot plant data. *Computers & Chemical Engineering*, 1992, 16: S441–S447
 60. Mullin J. *Crystallization*. 4th ed. Oxford: Butterworth-Heinemann, 2001, 141–160
 61. *Stream Analyzer OLI*. Version 11.5. OLI Systems Inc.: Parsippany, NJ, 2024
 62. Parkhurst D L, Appelo C A J. Description of input and examples for PHREEQC version 3—a computer program for speciation, batch-reaction, one-dimensional transport, and inverse geochemical calculations. In: *U.S. Geological Survey Techniques and Methods*. Reston: Geological Survey, 2013
 63. Puigdomenech I. *MEDUSA—Make Equilibrium Diagrams Using Sophisticated Algorithms*. Stockholm: KTH Royal Institute of Technology, 2022
 64. Chen X, Xu B, Zhou T, Liu D, Hu H, Fan S. Separation and recovery of metal values from leaching liquor of mixed-type of spent lithium-ion batteries. *Separation and Purification Technology*, 2015, 144: 197–205
 65. Pagnanelli F, Moscardini E, Altimari P, Abo Atia T, Toro L. Cobalt products from real waste fractions of end of life lithium ion batteries. *Waste Management*, 2016, 51: 214–221
 66. Peng C, Chang C, Wang Z, Wilson B P, Liu F, Lundström M. Recovery of high-purity MnO_2 from the acid leaching solution of spent Li-ion batteries. *Journal of the Minerals Metals & Materials Society*, 2020, 72(2): 790–799
 67. Vieceli N, Nogueira C A, Guimarães C, Pereira M F C, Durão F O, Margarido F. Hydrometallurgical recycling of lithium-ion batteries by reductive leaching with sodium metabisulphite. *Waste Management*, 2018, 71: 350–361
 68. Parween R, Rani K, Panda R, Sharma A, Ambade B, Kumar Jha M. Hydrometallurgical separation and purification to recover iron (Fe), copper (Cu), nickel (Ni), lithium (Li), cobalt (Co), and manganese (Mn) metals from the leach liquor of discarded LIBs. *Separation and Purification Technology*, 2025, 364: 132325
 69. Keller A, Hlawitschka M W, Bart H J. Application of saponified D2EHPA for the selective extraction of manganese from spent lithium-ion batteries. *Chemical Engineering and Processing*, 2022, 171: 108552
 70. Strauss M L, Diaz L A, McNally J, Klaehn J, Lister T E. Separation of cobalt, nickel, and manganese in leach solutions of waste lithium-ion batteries using Dowex M4195 ion exchange resin. *Hydrometallurgy*, 2021, 206: 105757
 71. Beak M, Park J, Park S, Jeong S, Kang J, Choi W, Yoon W S, Kwon K. Understanding the effect of nonmetallic impurities in regenerated cathode materials for lithium-ion battery recycling by tracking down impurity elements. *Journal of Hazardous Materials*, 2022, 425: 127907
 72. Wang D, Li W, Rao S, Tao J, Duan L, Zhang K, Cao H, Liu Z. Oxygen-free calcination for enhanced leaching of valuable metals from spent lithium-ion batteries without a reductant. *Separation and Purification Technology*, 2021, 259: 118212
 73. Joo S H, Shin S M, Shin D, Oh C, Wang J P. Extractive separation studies of manganese from spent lithium battery

- leachate using mixture of PC88A and Versatic 10 acid in kerosene. *Hydrometallurgy*, 2015, 156: 136–141
74. Yang Y, Xu S, He Y. Lithium recycling and cathode material regeneration from acid leach liquor of spent lithium-ion battery via facile co-extraction and co-precipitation processes. *Waste Management*, 2017, 64: 219–227
 75. Veceli N, Reinhardt N, Ekberg C, Petranikova M. Optimization of manganese recovery from a solution based on lithium-ion batteries by solvent extraction with D2EHPA. *Metals*, 2021, 11: 1–20
 76. Li J, Yang X, Fu Y, Huang H, Zhong Z, Wang Y. Recovery of Fe, Mn, Ni, and Co in sulfuric acid leaching liquor of spent lithium ion batteries for synthesis of lithium ion-sieve and $\text{Ni}_x\text{Co}_y\text{Mn}_{1-x-y}(\text{OH})_2$. *Hydrometallurgy*, 2019, 190: 105190
 77. Roa A, Butylina S, López J, Luis Cortina J, Virolainen S, Mänttari M. Lithium recovery from battery waste leachate by nanofiltration: impact of types of leaching acid and alkaline on permeability of lithium ions. *Separation and Purification Technology*, 2025, 360: 130821
 78. Li J, Yang X, Yin Z. Recovery of manganese from sulfuric acid leaching liquor of spent lithium-ion batteries and synthesis of lithium ion-sieve. *Journal of Environmental Chemical Engineering*, 2018, 6(5): 6407–6413
 79. Beak M, Park S, Kim S, Park J, Jeong S, Thirumalraj B, Jeong G, Kim T, Kwon K. Effect of Na from the leachate of spent Li-ion batteries on the properties of resynthesized Li-ion battery cathodes. *Journal of Alloys and Compounds*, 2021, 873: 159808
 80. Stephan E F, Miller P D. Solubility of lithium hydroxide in water and vapor pressure of solutions of lithium hydroxide above 220 °F. *Journal of Chemical & Engineering Data*, 1959, 7(4): 501–505
 81. Sokolowski T. Physical properties of aqueous solution of sodium sulphate. *Journal of Crystal Growth*, 1981, 52: 829
 82. Barrett C A, Evans E B. Solid solubility and lattice parameter of NiO-MnO. *Journal of the American Ceramic Society*, 1964, 47(10): 533
 83. Talik E, Załóg A, Skrzypek D, Guzik A, Zajdel P, Michalska M, Lipińska L. LiMn_2O_4 nanocrystalline electrode materials. *Crystal Research and Technology*, 2012, 47(3): 351–362
 84. Yang Y, Huang G, Xie M, Xu S, He Y. Synthesis and performance of spherical $\text{LiNi}_x\text{Co}_y\text{Mn}_{1-x-y}\text{O}_2$ regenerated from nickel and cobalt scraps. *Hydrometallurgy*, 2016, 165: 358–369
 85. Thierry V, Bou Farhat H. Lithium-bearing minerals under the scanning electron microscope equipped with energy dispersive spectrometry: challenges, recent advances, and prospects. *Chemical Geology*, 2023, 633: 121573
 86. Xiaobing L, Holland J, Burgess S, Bhadare S, Yamaguchi S, Birtwistle D, Statham P, Rowlands N. Detection of Lithium X-rays by EDS. *Microscopy and Microanalysis*, 2013, 19(S2): 1136–1137
 87. Park S, Ku H, Lee K J, Song J H, Kim S, Sohn J, Kwon K. The effect of NH_3 concentration during Co-precipitation of precursors from leachate of lithium-ion battery positive electrode active materials. *Journal of the Korean Institute of Resources Recycling*, 2015, 24(6): 9–16
 88. Warman J F, Karunawan J, Floweri O, Suryadi P N, Santosa S P, Iskandar F. Revealing the dual role of ammonia in the hydroxide Co-precipitation synthesis of cobalt-free nickel-rich $\text{LiNi}_{0.9}\text{Mn}_{0.05}\text{Al}_{0.05}\text{O}_2$ (NMA955) cathode materials for lithium-ion batteries. *Chemistry*, 2024, 202025: 20
 89. Tang M, Qiu L, Deng Y, Zhang M, Guo F, Pang Q, Zhong B, Song Y, Guo X. Revealing the role of ammonia in the rapid crystallization kinetics for Ni-rich hydroxide precursors via microreactors. *Industrial & Engineering Chemistry Research*, 2024, 63(51): 22411–22421
 90. Purwanto A, Fajar A, Mugirahardjo H, Fergus J W, Wang K. Cation distribution in spinel $(\text{Mn}, \text{Co}, \text{Cr})_3\text{O}_4$ at room temperature. *Journal of Applied Crystallography*, 2010, 43(3): 394–400
 91. Wijnhorst R, Demmenie M, Jambon-Puillet E, Ariese F, Bonn D, Shahidzadeh N. Softness of hydrated salt crystals under deliquescence. *Nature Communications*, 2023, 14(1): 1090
 92. Yu Y, Rui X, Wu M. Sodium Systems—Low Temperature (LIB equivalent) Sodium-Ion Batteries: Alternative to Lithium-Ion Batteries. In: *Reference Module in Chemistry, Molecular Sciences and Chemical Engineering*. Amsterdam: Elsevier, 2025
 93. Yuan M, Liu H, Ran F. Fast-charging cathode materials for lithium & sodium ion batteries. *Materials Today*, 2023, 63: 360–379
 94. Milian Y E, Jamett N, Cruz C, Herrera-León S, Chacana-Olivares J. A comprehensive review of emerging technologies for recycling spent lithium-ion batteries. *Science of the Total Environment*, 2024, 910: 168543
 95. Liang J, Chen R, Gu J, Li J, Xue Y, Shi F, Huang B, Guo M, Jia J, Li K, et al. Sustainable recycling of spent ternary lithium-ion batteries via an environmentally friendly process: selective recovery of lithium and non-hazardous upcycling of residue. *Chemical Engineering Journal*, 2024, 481: 148516